

Fundamental optoelectronic processes in amorphous chalcogenides

K. Shimakawa, Y. Ikeda, S. Kugler^a

*Department of Electrical and Electronic Engineering, Gifu University,
Gifu 501-1193, Japan*

*^aBudapest University of Technology and Economics, H-1521 Budapest,
Hungary*

Amorphous chalcogenides reveal characteristic optoelectronic natures. The photo-induced effects on these properties are of particular interest from the viewpoints of fundamental science and applications. In the present chapter, current understandings of these optoelectronic properties in amorphous chalcogenides are briefly reviewed.

Introduction

Although a great number of studies have been undertaken to understand the characteristics of electronic and optical properties of amorphous semiconductors in the last three decades, many of these properties are still not clear. It is well known that amorphous chalcogenides show a metastable photoinduced transformation of structural network and microscopic defect structures [1-5]. Some of these properties are fairly well understood, while some are still matter of debate.

In this chapter, we first discuss the fundamental optical and electronic transport properties, which cannot be interpreted by a standard model used in crystalline semiconductors. It will be noticed that conventional models for explaining the optical and electronic properties cannot be applied for some of amorphous chalcogenides [6,7]. Then, we review the current understanding of photoinduced effects, in particular the light induced defect (LIMD) creation and the photoinduced structural changes (PSC) observed in amorphous chalcogenides.

Fundamental optical properties and electronic transport

Fundamental optical absorption

The analysis of optical absorption spectra is one of the most useful tools for understanding the electronic structure of amorphous semiconductors. As found in a free electron gas, it is expected that the density-of-states (DOS) for both conduction and valence bands is proportional to the square root of the energy in 3D materials. This leads to the well known Tauc plot for the optical absorption coefficient α as a function of photon energy $\hbar\omega$ giving $(\alpha\hbar\omega)^{1/2} \propto (\hbar\omega - E_o)$, where E_o is the optical gap which is a measure of the bandgap in amorphous solids [8]. However, this quadratic energy dependence of the absorption coefficient on photon

energy is not always observed; e.g. a linear energy dependence for amorphous Se (a-Se) and a cubic energy dependence for multicomponent chalcogenide glasses have been observed [9]. The deviation from the simple Tauc relation may be regarded to arise from the derivation of DOS from a simple power law.

The DOS in disordered matters, in general, should be described by taking into account the *fractals* that are known to dominate many physical properties in amorphous semiconductors [10,11]. We revisit the classical problem for interpreting optical properties of amorphous semiconductors on the basis of the form of DOS applicable to amorphous chalcogenides. We find that the fundamental optical absorption in amorphous chalcogenides can be written as $(\alpha\hbar\omega)^n \propto (\hbar\omega - E_0)$, where the value of n deviates from $1/2$. Typical examples are shown in Figs. 1 and 2 for obliquely deposited amorphous As_2S_3 and Se (hereafter a- As_2S_3 and a-Se), which are given in the plot of $(\alpha\hbar\nu)^n$ vs. $\hbar\nu$, respectively which are given in the plot of $(\alpha\hbar\nu)^n$ vs. $\hbar\nu$ [6]. The fitting to the experimental data for a- As_2S_3 (Fig. 1 (a) and (b)) produces $n = 0.70$ before annealing (as deposited) and $n = 0.59$ after annealing near the glass transition temperature for film. Note that similar values of n (0.73 for as deposited and 0.58 after annealing) for a- As_2Se_3 are obtained [6]. The fitting to the data for a-Se (Fig. 2) produces $n=1$ for a-Se before annealing (as deposited) and this behavior is unchanged after annealing at 30°C for 2 hr.

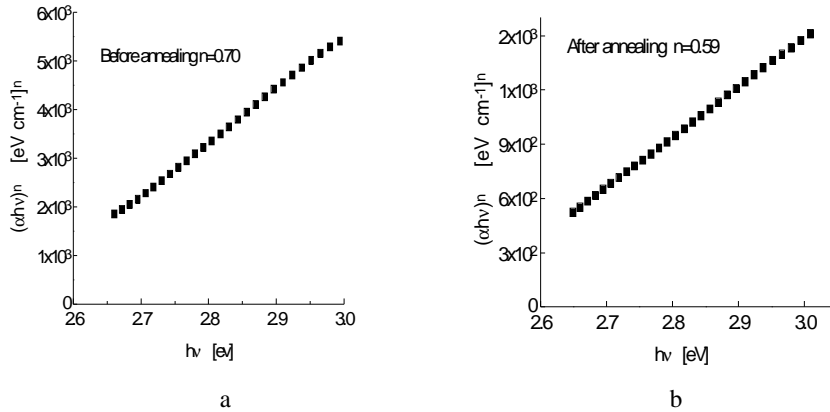


Fig. 1. Optical absorption spectra plotted for $(\alpha\hbar\nu)^{1/2}$ vs. $\hbar\nu$ in obliquely deposited a- As_2S_3 . (a) $n = 0.70$ before annealing and (b) $n = 0.59$ after annealing at 170°C for 2 hr.

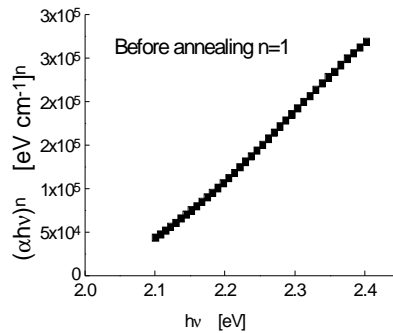


Fig. 2. Optical absorption spectra plotted for $(\alpha\hbar\nu)^{1/2}$ vs. $\hbar\nu$ in obliquely deposited a-Se. $n = 1$, which remains unchanged before and after

annealing.

Here, a brief derivation of the fundamental optical absorption coefficient is given to facilitate the interpretation of the experimental results given above. For interband electronic transition the optical absorption coefficient under some conventional assumptions can be given as

$$\alpha(\omega) = B \int \frac{N_v(E)N_c(E + \hbar\omega)dE}{\hbar\omega}, \quad (1)$$

where B is a constant and the integration is over all pairs of states in the valence states $N_v(E)$ and the conduction states $N_c(E)$. If the density of states for the conduction and valence states are assumed to be $N_c(E)=\text{const} (E-E_A)^s$ and $N_v(E) = \text{const} (E_B - E)^p$, respectively, then Eq.(1) produces

$$\alpha(\omega)\hbar\omega = B'(\hbar\omega - E_o)^{p+s+1}. \quad (2)$$

This gives

$$[\alpha(\omega)\hbar\omega]^n = B'^{\frac{1}{n}} (\hbar\omega - E_o), \quad (3)$$

where $1/n=p+s+1$. If the form of both $N_c(E)$ and $N_v(E)$ is parabolic, i.e. $p = s = 1/2$ for 3 D, then the photon energy dependence of the absorption coefficient obtained from Eq.(3) becomes

$$[\alpha(\omega)\hbar\omega]^{\frac{1}{2}} = B'^{\frac{1}{2}} (\hbar\omega - E_o). \quad (4)$$

Let us first discuss a simple case of a-Se. The sum of $(p + s)$ should be zero for $n=1$ in a-Se. This is only possible if the product of DOS is independent of the energy. The origin for this was argued long time ago but was unclear [9]. A chain-like structure is basically expected in a-Se. The top of the valence states is known to be formed by p-lone pair (LP) orbitals (lone pair interaction) of Se atoms. The interaction between lone pair electrons should have 3D in nature and therefore the parabolic DOS near the V.B. edge can be expected, i.e. $p=1/2$. The bottom of the conduction states, on the other hand, is formed by anti-bonding states of Se. If the interaction between chains is ignored, the DOS near the conduction states may have 1D nature, i.e. $s=-1/2$. We hence obtain $n = 1/(p + s + 1) = 1$, producing linear dependence of energy, i.e. $(\alpha\hbar\omega) \propto (\hbar\omega - E_o)$.

Next, we discuss the $\text{As}_2\text{S}(\text{Se})_3$ binary systems. These systems are suggested to have layered structures [12, 13]. The top of valence states are formed by the LP band and the parabolic DOS near V.B. can be expected also in these systems, since LP-LP interactions occur in 3D space as already mentioned. Unlike a-Se, the bottom of C.B. basically should arise from a 2D structure in nature, if the layer-layer interactions can be ignored for anti-bonding states (C.B.). This means that the corresponding DOS is independent of energy ($s=0$). The value of n , in this case, should be given by $2/3$, since $p = 1/2$ and $s = 0$ are predicted from the argument of space dimensions, and it is close to those observed for as-deposited oblique films of a- $\text{As}_2\text{S}(\text{Se})_3$. It should be noted, however, that the layer-layer interactions cannot be ignored for the DOS of C.B. [14].

The deviation from $n = 2/3$ or $n = 1/2$ may be attributed to the fractional nature in the DOS; i.e. p or s cannot be given as just $1/2$ (3D), 0 (2D), and $-1/2$

(1D). In obliquely deposited As_2Se_3 , for example, $n=0.70$ (before annealing) produce $p + s = 0.43$. For interpreting these results, we may need to discuss the DOS for fractal structures. The DOS for the extended states on d -space dimension in usual Euclid space is given as

$$N(E)dE \propto \rho^{d-1}d\rho, \quad (5)$$

where ρ is defined as $(2m^*E)^{1/2}/\hbar$, instead of the wave vector k , since k is not a good quantum number in disordered matters and m^* is the effective mass [15]. On fractal space, on the other hand, a fractal dimension D is introduced, instead of d [10]. The DOS for the extended states on fractal space D can be given by [10]

$$N(E)dE \propto \rho^{D-1}d\rho \propto E^{\frac{D-2}{2}}dE. \quad (6)$$

Note that D is introduced as $M(r) \propto r^D$, where M is the “mass” in a space, and hence D can take any fractional value (even larger than 3). A similar argument of fractional dimensionality on interband optical transition has also been presented in anisotropic crystals applicable to low dimensional structures [16].

As we discussed already the energy dependence of DOS for the C.B. is expected to be different from that for the V.B. in amorphous chalcogenides, but usually the space dimensionality for V.B. is larger than that for C.B. Therefore, we introduce D_v and D_c for the dimensionality of V.B. and C.B., respectively. Then $p + s + 1$ in Eq.(2) is replaced by

$$p + s + 1 = \frac{D_v + D_c - 2}{2}, \quad (7)$$

for fractional dimension systems. From the value of $n (=2/(D_v + D_c - 2))$, $D_v + D_c$ can be deduced. In As_2S_3 , for example, $D_v + D_c$ is 4.86. After thermal annealing, the value of n tends to 0.5 for both the oblique and flat samples ($D_v + D_c \approx 6$), indicating that each D_v and D_c approach 3-dimension. This is due to the fact that thermal annealing produces more ordered and dense structural network. The similar argument has been also given for flatly deposited materials [6].

A cubic energy dependence, $n = 1/3$, is often observed for multicomponents (e.g. Ge-As-Te-Si), and $D_v + D_c = 8$ is obtained for $n = 1/3$. This higher fractal dimension may be related to “branching” or “cross-linking” between Te chains by introducing As, Ge, and Si atoms [11]. The “branching” may be equivalent to “Bethe lattice (or Cayley tree), resulting in an increase in space dimension [10,11].

Now, let us summarize the fundamental optical absorption in amorphous chalcogenides. The fundamental optical absorption, empirically presented by the relation $(\alpha\hbar\omega)^n \propto (\hbar\omega - E_0)$, where n is deviated from 1/2, in amorphous chalcogenides was interpreted by introducing the density-of-states (DOS) on fractals. The energy-dependent DOS form is not the same between C.B. and V.B. The presence of disorder can greatly influence the nature of the electronic density of states (DOS) even for the extended states. The concept of DOS on the fractal structures was successfully applied to interpret the fundamental optical absorption spectra.

Finally, we should discuss briefly the validity of Eq.(1) in which the transition matrix element is implicitly assumed to be independent of energy; i.e. B

is independent of energy. Dersh et al. [17], on the other hand, suggested that the transition matrix element is energy-dependent and has a peaked nature near the bandgap energy. More detailed discussed may be required.

Electronic transport

It is known that free holes dominate the electronic transport at relatively high temperatures in amorphous chalcogenides. It is then expected that the electric conductivity is expressed by standard band-transport model. However, as described below, the conductivity is found to obey the Meyer-Neldel rule (MNR),

$$\sigma = \sigma_0 e^{-\Delta E/kT}, \quad (8)$$

and the prefactor correlates with the activation energy ΔE as

$$\sigma_0 = \sigma_{00} e^{\Delta E/E_{MN}}, \quad (9)$$

where σ_{00} is a constant and E_{MN} is often called as the Meyer-Neldel characteristic energy [7]. Note that the σ_0 should take a constant value in the standard transport model. The MNR, or compensation law, is known to apply to various thermally activated phenomena, e.g. kinetics (hopping) and thermodynamics (number of carriers in the band states), in crystalline, amorphous, and liquid semiconductors [18-21].

Although numerous experimental data have been presented for the case of a-Si:H [22], no attention has been paid to chalcogenide glasses. Shimakawa and Abdel-Wahab [7], taking Borisova's numerous data [23], have found evidence for the NMR in many chalcogenide glassy systems. One of the examples obeying the NMR is shown in Fig. 3 for the As-Se-S system. The solid line represents the best fit to the experimental data, which produces the values of σ_{00} ($1.0 \times 10^{-15} \text{ S cm}^{-1}$) and E_{MN} (28 meV). We know that E_{MN} lies in the range of 25 - 60 meV and σ_{00} in the range of $10^{-5} - 10^{-15} \text{ S cm}^{-1}$ for some of the examined systems. Note that σ_{00} and E_{MN} for a-Si:H lie around 1 S cm^{-1} and 40 meV, respectively.

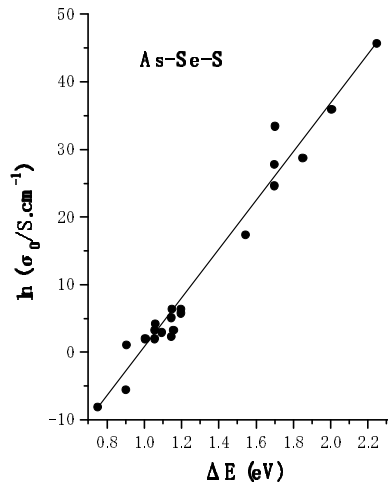


Fig. 3. The correlation between σ_0 and E_{MN} in the As-Se-S system.

The prefactor, σ_0 , itself is not regarded as microscopic conductivity ($e\mu_0N_v$), where μ_0 is the microscopic mobility and N_v the effective density-of-states in the relevant band (valence band in chalcogenide glasses), since a large scatter of σ_0 is not easy to explain by the standard band-transport model. Instead, σ_{00} may have physical meaning in terms of a microscopic conductivity ($\sigma_{00} = e\mu_0N_v$). The very small magnitude of σ_{00} , as compared with that ($\approx 1 \text{ S cm}^{-1}$) in a-Si:H, suggests that the conduction mechanism in chalcogenides may not be the same as that in a-Si:H. Note that σ_{00} in a-Si:H is close in value to the microscopic conductivity ($e\mu_0N_v$) for standard model.

Small-polaron hopping has been suggested to dominate the dc transport in chalcogenide glasses [24]. In fact, as a unified model, multiphonon excitations have been suggested for the MNR in condensed matter [19,20]. In this model, the magnitude of σ_{00} is predicted to be $10^2 - 10^3 \text{ S cm}^{-1}$ for small polaron, which is very much larger than the experimentally obtained prefactors ($10^{-5} - 10^{-14} \text{ S cm}^{-1}$). The small-polaron model seems unable to explain the dc transport in chalcogenide glasses.

The NMR is also found in organic semiconductors [25], in which similar small values of σ_{00} ($10^{-3} - 10^{-17} \text{ S cm}^{-1}$) have been found. The electronic transport in organic semiconductors may be dominated by tunneling of electrons through intermolecular barriers and hence the tunneling factor which should depend on the potential barrier should be included in the prefactor in the conductivity [7]. The small prefactor is thus attributed to a small tunneling factor. A similar situation, phenomenologically, may occur in chalcogenide glasses. Most chalcogenide glasses have two dimensional (2D)-like layered structures and hence the carriers must cross interlayer potential barriers, since the transport occurs in 3D space. Thus the prefactor σ_{00} is very small. This means that $e\mu_0N_v$ in the 3D expression becomes effectively small in chalcogenide glasses.

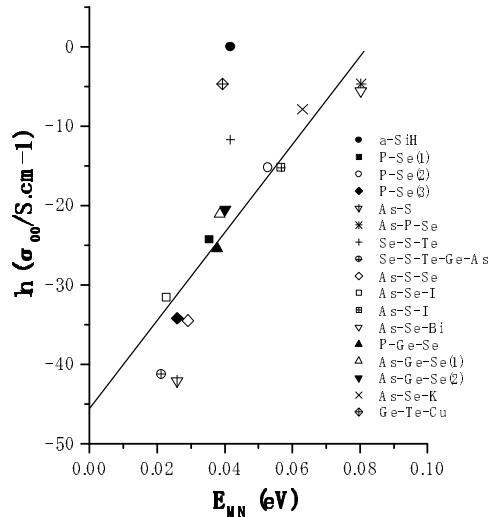


Fig. 4. The correlation between σ_{00} and E_{MN} for some chalcogenide glasses. The closed circle represents the datum for a-Si:H for

comparison.

A surprising correlation between σ_{00} and EMN has been found in chalcogenide glasses as shown in Fig. 4 and is given by the following empirical relation:

$$\sigma_{00} = \sigma'_{00} e^{E_{MN}/\varepsilon}, \quad (10)$$

where ε is a constant (1.7 meV).

In summary, the NMR is found to be obeyed in some chalcogenide glasses. The magnitude of the prefactor, σ_0 , itself estimated from the Arrhenius plot, does not have any physical meaning. Instead, σ_{00} , should have physical meaning. Interlayer tunneling of holes, which yield a small magnitude of prefactor (σ_{00}), unlike in a-Si:H, may dominate the dc transport. The origin of the NMR together with the surprising correlation given by eq.(10) is not clear at present.

Photo-induced transformations of physical properties

Two types of reversible photoinduced effects are well known in amorphous chalcogenides, namely the structural changes and defect creation. These photoinduced changes are returned to their original states by thermal annealing. Although these reversible changes have been discussed in numerous papers, its microscopic origin is still not clear [1-5].

The photoinduced defect creation first has been found in hydrogenated amorphous silicon (a-Si:H) and has been found later also in amorphous chalcogenides (see, for example, ref.[1]). Such defect creation affects device applications, because such defects act as recombination centers, and hence these should be removed or minimized. In spite of great effort to overcome this degradation, it is still a difficult problem. Flexible or deformable structural network in amorphous materials may facilitate such degradation and self-trapped exciton (STE) states are considered to be a candidate of inducing defects [1].

Photostructural change (PSC) and the related photodarkening (PD) are phenomena unique to glassy or amorphous chalcogenides (a-Chs) and are not observed in amorphous group IV and V semiconductors (a-Si, a-As etc.), or in crystalline chalcogenides [1]. These effects can be useful for optical memory applications.

In the present section, interesting results recently obtained on the defect creation (in particular, quantum efficiency), reversible PD and PVE for As-based chalcogenides are reviewed. We will concentrate to the time evolution of these changes (*in situ* measurements etc.), which is useful in understanding the dynamics of defect creation, PD, and PVE.

Photo-induced defect creation

The self-trapped exciton (STE), which requires a strong carrier-lattice interaction, may play an important role for light-induced metastable defect (LIMD) creation in amorphous chalcogenides [1]. In the STE model, the primary optical excitation event itself is assumed to be the origin of LIMD creation and subsequent non-radiative recombination (multiphonon process) assists their stabilization.

We concentrate here the LIMD creation only. All kinetic equations proposed so far have discussed the time evolution of LIMDs. The dependence of

the number of created defects N on the total number of absorbed photons $n_p (= Gt)$ will be discussed here [2,6,26]. We define the quantum efficiency of LIMD creation as $\eta = N(n_p)/n_p$. The quantum efficiency of LIMD creation as a function of total number of absorbed photons is estimated and these results can be explained by the rate equation for defect creation. It is of interest to know how QE depends on n_p and on the photon energy in the LIMD creation. We also discuss the effect of structural flexibility on QE. To observe the effect of structural flexibility, we have studied LIMD creation during illumination by measuring photocurrent with time for normal and obliquely deposited $a\text{-As}_2\text{Se}_3$ films.

Fig. 5 shows the experimentally obtained photocurrent I_p as a function of exposure time t at 300 K and 250 K for (a) bandgap and (b) sub-bandgap illuminations, respectively. The symbols used are described in the figure caption. The solid lines are calculated results, which will be discussed later. For bandgap illumination, the photocurrent I_p decreases with time and approaches a minimum and then increases for both the obliquely and normally deposited films. In obliquely deposited films I_p is comparatively lower than for normally deposited films. For sub-bandgap illumination, no pronounced decrease in I_p is observed. I_p decreases very slowly, and does not show any increase even after two hours of illumination as in the case of band gap illumination. A decrease in photocurrent could result from the photoinduced creation of recombination centers (defects).

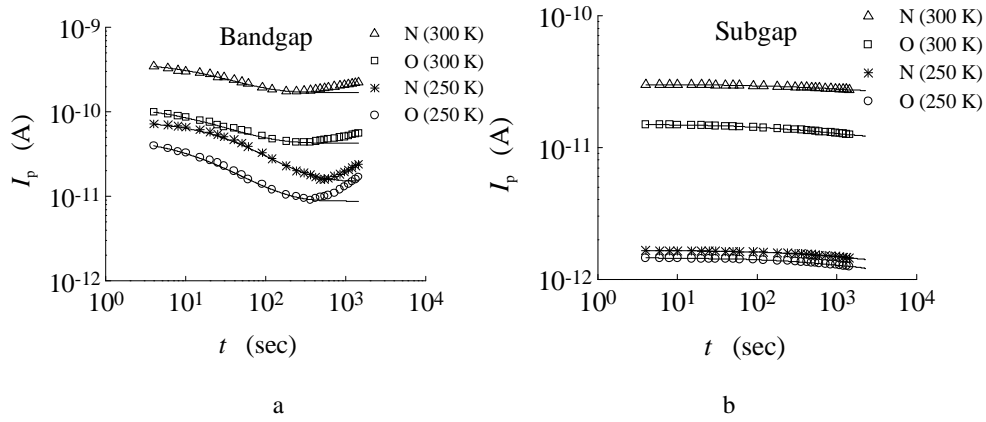


Fig. 5. Variation of photocurrent with exposure time measured at 300 K and 250 K for $a\text{-As}_2\text{Se}_3$ films for (a) bandgap illumination, and (b) sub-gap illumination. N and O represent normally and obliquely deposited films, respectively. Solid curves are calculated results (see the text).

In a microscopic model for LIMD creation, Shimakawa et al.[1,27,28] proposed that the creation of widely separated random pairs (RPs) of positively and negatively charged centers is responsible for the decrease in the photocurrent. Such RPs results from defect-conserved bond-switching reactions at optically induced intimate pairs (IPs). For sub-bandgap illumination (Fig. 5(b)), we may expect that the number of RP center is smaller, resulting in a smaller decrease of I_p .

The increase in photocurrent I_p for band gap illumination shown in Fig.

5(a) can be caused by the increase of optical absorption due to photodarkening (PD), which can be responsible for the increase in the number of photo-excited carriers [29]. The magnitude of the change of increasing photocurrent at 250 K is greater than that at 300 K, suggesting that the PD at 250 K is bigger than at 300 K. This is in accordance with the recent observation of illumination-time and temperature dependence of PD, which will be discussed in the following section.

Now we discuss the defect creation N_t during illumination. It is assumed here that change in the photocurrent is dominated by LIMD creation itself. The photocurrent, under conditions of thermal equilibrium, with exposure time can be expressed as

$$I_p(t) = \frac{C}{N_0 + N_t} = \frac{C}{N_0(1 + N_t/N_0)} = \frac{I_p(0)}{1 + N_t/N_0}, \quad (11)$$

where C is a constant and $I_p(0) (=C/N_0)$ is the initial photocurrent. N_t/N_0 can be estimated from the ratio $I_p(0)/I_p(t)$, with N_0 being the initial number of defects in the film. Fig. 6 shows the variation of defect creation (N_t/N_0), for (a) bandgap and (b) sub-gap illuminations, respectively, with exposure time estimated from the changes in photocurrent using Eq. (1). All symbols are given in the figure caption. The solid lines are calculated results, which will be discussed later. N_t increases with time during illumination in obliquely and normally deposited films. It is clear that N_t for obliquely deposited films is always larger than that for normally deposited ones at the same temperature. From this observation it is suggested that the LIMD creation is more enhanced in obliquely deposited samples than in normally deposited ones. Large structural flexibility in obliquely deposited films may show large LIMD creation.

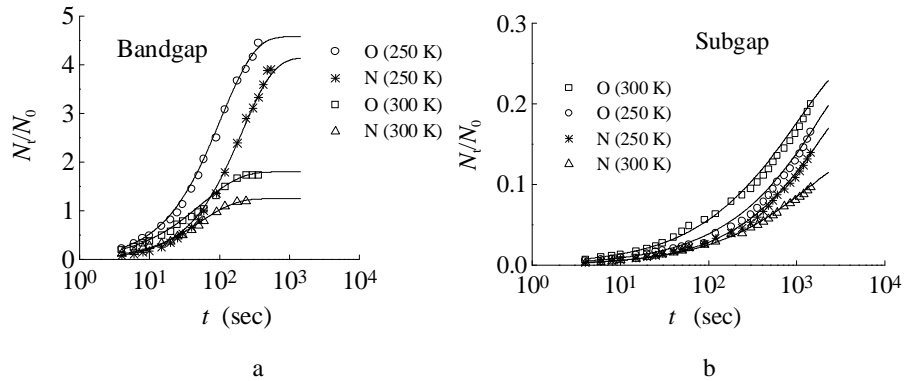


Fig. 6. Variation of N_t/N_0 with exposure time, which is estimated from the changes in photocurrent for (a) bandgap and (b) sub-gap illumination. Description of symbols is the same as in Fig. 5. Solid lines are the fitting obtained using Eq. (13).

Although various kinetic models for LIMD creation have been proposed, we take the following rate equation for LIMD creation [1]:

$$\frac{dN_t}{dt} = k_p(N_T - N_t) - k_r N_t, \quad (12)$$

where N_T is the total potential sites for LIMD creation, k_p and k_r being the promotion and recovery rate, respectively. Assuming a time dispersive reaction for promotion and recover reactions as $k_p = At^{\alpha-1}$ and $k_r = Bt^{\alpha-1}$, respectively, where A and B are constant, the number of defects, N_t created during illumination is given as

$$N_t = N_s \left[1 - \exp \left\{ - \left(\frac{t}{\tau} \right)^\alpha \right\} \right], \quad (13)$$

where $N_s = N_T A / (A+B)$ is the saturated density of N_t and $\tau = [\alpha / (A+B)]^{1/\alpha}$ is the effective creation time. Here the dispersion parameter α ($0 < \alpha < 1$) is assumed to be the same for both the forward and backward reactions. From Eq. (13) we can evaluate N_t/N_0 [dividing Eq. (13) by N_0] as a function of illumination time by assuming the parameter N_s/N_0 .

Using Eqs. (11) and (13) the photocurrent can be written as

$$I_p = \frac{I_s}{1 - \gamma \exp \left\{ - \left(t / \tau \right)^\alpha \right\}}, \quad (14)$$

where I_s is a constant current reached by prolonged illumination and $\gamma = N_s / (N_0 + N_s)$. The solid lines in Figs. 5 and 6 are calculated results by using α , τ , and N_s/N_0 (or γ) as the fitting parameters. The fittings to the experimental data are reasonably good and these parameters are tabulated in the table. The following conclusions can be drawn: For both bandgap and sub-gap illuminations, and for the same temperature at which illumination was made, the values of N_s/N_0 and γ for the obliquely deposited samples are larger than those for the normal ones. The effective creation time τ for the sub-gap illumination is larger than that for bandgap illumination and it increases with decreasing temperature. The dispersion parameter α is smaller for sub-gap illumination than that for bandgap illumination.

Table. Fitting parameters obtained using equation (16). $\Delta\alpha_s$ is the saturated value of change in optical absorption, τ the effective reaction time, and β the dispersion parameter.

	Bias condition		
	Positive on ITO	Negative on ITO	Zero
$\Delta\alpha_s$ (cm ⁻¹)	1700	1700	1600
τ (s)	2000	4200	5500
β	0.40	0.60	0.90

We now define the quantum efficiency (QE) η of LIMD creation, which is defined as

$$\eta = N_t / n_p, \quad (15)$$

where N_t is the number of defects created by illumination and n_p is the total number of absorbed photons. To get N_t we need to know the value of N_0 . Here, the value of N_0 is assumed to be $1 \times 10^{17} \text{ cm}^{-3}$ [1, 26]. Total number of absorbed photons n_p is evaluated as $n_p = Gt$, where t is the illumination time and G is the rate of absorbed photons ($\text{cm}^{-3} \text{ sec}^{-1}$). Fig. 7 shows the QE, η , as a function of total number of absorbed photons n_p for (a) bandgap and (b) sub-gap illuminations, where again symbols are given in figure caption.

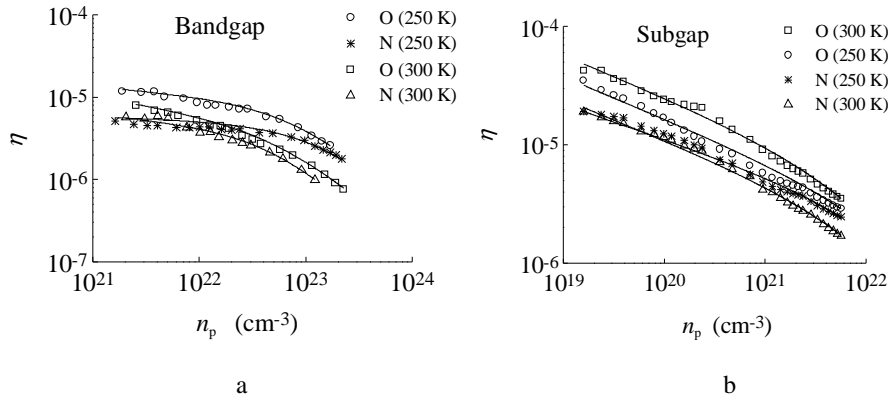


Fig. 7. Variation of quantum efficiencies η with the number of absorbed photon n_p for (a) bandgap and (b) sub-gap illumination. Description of symbols is the same as in Fig. 5. Solid lines are calculated results using Eq.(15).

It is shown that the QE decreases with increasing number of absorbed photons for both the bandgap and sub-bandgap illumination. At the studied temperatures, all the results show a similar behavior. The solid lines in Fig. 7 represents the calculated results of QE using Eqs. (13) and (15), which are also in good agreement with the experimental results. Fig. 8 shows the comparison of QEs in obliquely and normally deposited films for (a) band gap and (b) sub-band gap illuminations at studied temperatures (300 K, 250 K). All symbols used are described in the figure caption. At 300K the variation of quantum efficiency with number of absorbed photons is nearly parallel to each other for both band gap and sub-band gap illumination (Fig. 8(a)), but at 250 K this variation is not clear (Fig. 8(b)). At both temperatures QE is larger in obliquely than normally deposited films.

The QE at smaller n_p for subgap illumination seems to be larger than that for bandgap illumination. The difference between them, however, is within a factor of 2-3. As we used several free parameters for calculations, this difference may not have any significance. It is thus suggested that bandgap and sub-gap illuminations produce almost the same QE. As we expect intuitively that QE to be dependent on photon energy (higher photon energies are expected to create LIMDs more efficiently), this result is therefore somewhat surprising.

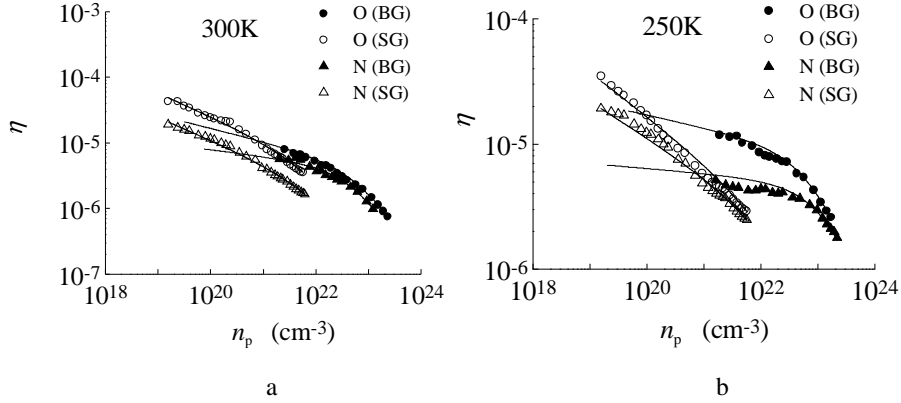


Fig. 8. Comparison of quantum efficiencies for bandgap and sub-gap illumination for obliquely and normally deposited films at (a) 300 K and (b) 250 K.

Although the mechanisms of LIMD creation are not clear, self-trapped exciton (STE) and/or non-radiative *multiphonon* [1, 30] recombination between electrons and holes which are localized relatively deep in tail states could only contribute to LIMD creation. Therefore, thermalization energy of photocarriers from the extended states to the tail states may not be important for LIMD creation, since thermalization from extended states to tail states may involve only the emission of *single* phonons, which is insufficient for LIMD creation. The STEs can be created easily by sub-gap illumination as well and hence QE for sub-gap illumination may be comparable for bandgap illumination.

In Fig. 9, data for both a-As₂Se₃ and a-Si:H are shown for comparison. The QE for a-As₂Se₃ is larger than that for a-Si:H. This can be attributed to the high degree of flexibility of the atomic structure in amorphous chalcogenides. It should be noted also for a-Si:H that bandgap and subgap illuminations produce almost the same QE. Probably, the same reason for a-As₂Se₃ can be applied to explain that for a-Si:H. In fact, self-trapped holes (STH) has been suggested to initiate LIMD creation in a-Si:H, in which sub-gap illumination also create STHs effectively [31,32].

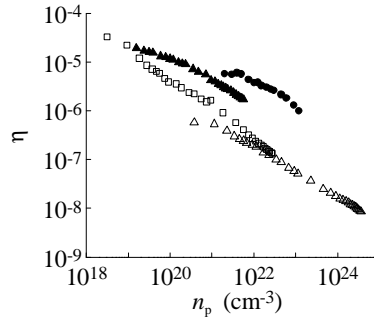


Fig. 9. Comparison of η for a-Si:H (Δ for bandgap and \square for sub-gap illumination) and a-As₂Se₃ (\bullet for bandgap and \blacktriangle for sub-gap illumination).

Finally, we should discuss the case for pulsed excitation. It is known that illumination of a-Si:H with short intense light pulses creates LIMDs much faster than cw irradiation with the *same average intensity* and photon energy [33]. Note also that the saturation concentration of LIMDs for pulsed excitation reaches 10^{18} cm^{-3} , which is much larger than that (10^{17} cm^{-3}) for cw excitation. This discrepancy may be due to highly non-equilibrium conditions under pulsed excitation. The kinetic equation (applied to equilibrium conditions in this paper) is not appropriate for pulsed excitation. It is of interest to perform such pulsed excitations for amorphous chalcogenides.

The discussions made above are phenomenological. Computer simulations can be helpful to get a microscopic view for LIMD creation. Tight-binding molecular dynamics (MD) simulations of photo-excitations in small Se clusters (isolated Se_8 ring and helical Se chain) and glassy networks (162 atoms) have been carried out in order to understand the photo-induced instability of amorphous chalcogenides [34,35]

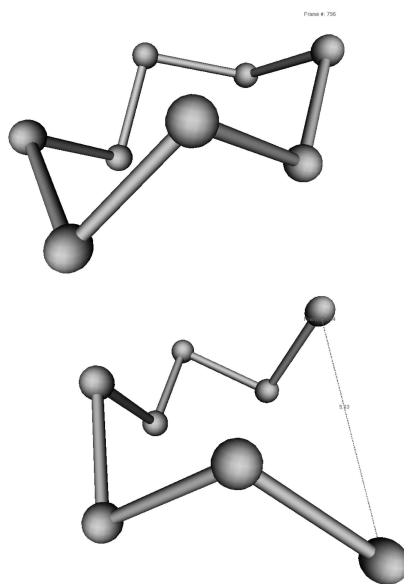
A MD computer code (ATOMDEP program package) has been developed to simulate the real preparation procedures of amorphous structures (grown by atom-by-atom deposition on a substrate and rapid quenching). Recently, the growth of amorphous carbon, silicon, and selenium was simulated by this MD method [35-38]. This computer code is convenient to investigate both the LIMD creation and photo-induced volume changes as well if the built-in atomic interaction can handle the photo-excitation. Standard velocity Verlet algorithm was applied in the MD simulations in order to follow the atomic scale motion. We chose $\Delta t = 1$ or 2 fs for the time step, depending on the temperature. These values are the typically used time steps for such simulations. To control the temperature of the systems the velocity-rescaling method is applied. For calculating the inter-atomic forces in a-Se we used the tight-binding (TB) [38] and self-consistent tight-binding (SCF-TB) models [40].

Two systems are employed as follows. (i) One is a cluster geometry: Crystalline forms of selenium consist of chains and eight-membered rings. Typical bond lengths are around 2.35 Å while most of the bond angle values are around 103° . It is very likely that these local arrangements can be found in non-crystalline forms of selenium as well. The initial configuration of the eight-membered ring in the simulation had bond lengths of 2.38 Å and bond angles of 102° . Dihedral angles are equal to 100° . For the eighteen-membered selenium chain (with 1-dimensional periodic boundary condition) these values are 2.36 Å, 100° , and 98° , respectively. Every Se atom has two first-neighbors, i.e. there is no coordination defect.

Before illumination (photo excitation) the individual ring and the chain were relaxed for 4 ps at $T = 500$ K. During this period the structures were stable. When a photon is absorbed an electron from the highest occupied molecular orbital (HOMO) to the lowest unoccupied molecular orbital (LUMO) is transferred. This is a simple model of photo-excitation when an electron is shifted from the valence band to the conduction band (electron-hole pair creation). In the present study, recombination of electron-hole pair was also simulated by taking back the electron from the conduction band to the valence band. The lifetime of the excitation was 200 fs.

After excitation one bond length in the ring started to increase and bond-breaking occurred. Two snapshots of this process can be seen in Fig. 10. A similar result was obtained for S_8 ring [41] in which a MD simulation within the framework of density functional theory in the local density approximation. For the

linear chain structure, the same procedure was performed to model the excitation. An electron from HOMO to LUMO was transferred. Very similar result was obtained as in the ring structure; a bond inside the chain is broken immediately after a HOMO electron was excited.



□ Fig. 10. Top panel is the ring structure before excitation. Bottom shows the configuration at 420 (fs) after excitation.

Of particular interest here is the following. Bond breaking occurs when lone pair electron (HOMO: forming the valence band in Se) is excited into LUMO (forming the conduction band). Note here that bonding electron is not excited ! It is therefore suggested that the occupation of electron in LUMO may result in bond breaking.

(ii) The other is a glassy system: Glassy selenium networks having 162 atoms (with three-dimensional periodic boundary conditions) were prepared by “cook and quench” technique (from 3000 to 20 K). The average quenching rate is 4×10^{12} K/s. After quenching the periodic boundary constraint in the z direction is released in the simulation and the system is allowed to relax for another 100 ps. In this way the system could change its volume in the z direction. Four models have been presented with different initial topologies and densities.

Next, we discuss the photo-induced effect on the glassy structure. The excitation procedure for the glassy networks was different from the method applied for small clusters. The whole procedure was carried out at the temperature of 20 K. Instead of a single electron excitation, five electrons were transferred from the valence band to the conduction band. The first excited electron was taken from the HOMO, the second excited electron was taken from the level below it and so on. Our systems were open only along the z direction and periodic boundary conditions were applied in the other two directions.

It is shown in this simulation that the number of coordinated defects are changed by illumination. Basically, selenium atoms have two nearest-neighbors. Average numbers of one-fold coordinated and threefold-coordinated atoms are shown in Fig. 11. Actually, the number of twofold coordinated atoms remained the same in our simulations. During illumination the number of one-coordinated defects was increased while it was opposite for threefold coordinated selenium atoms. During the de-excitation the inverse process occurred. It is striking that there are more threefold defects and less one-fold coordinated atomic sites at the end of the simulation compared to initial configuration. In this simulation, volume change has been also discussed [34,35] and photo-induced volume changes will be discussed in the next section.

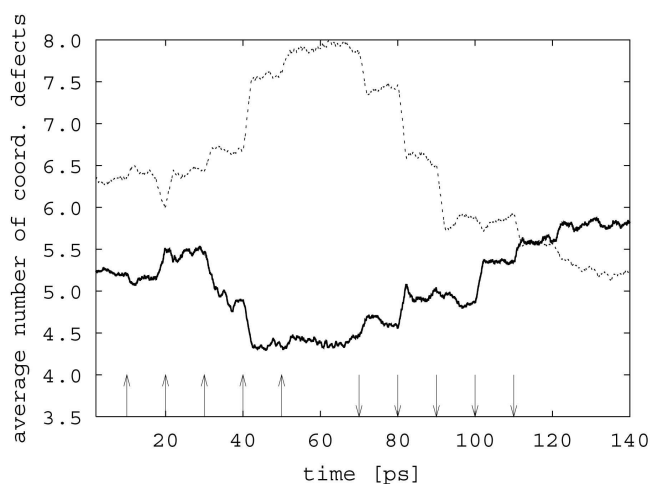


Fig. 11. Average numbers vs. time of one-fold coordinated (dashed line) and threefold-coordinated (solid line) atom glassy network.

Photo-induced volume changes

We start from the metastable changes in PD and PVE. It is observed that bandgap decreases and thickness increases by illumination and that giant changes are induced in obliquely deposited films [42,43]. It was believed for a long time that PD and PVE were two different sides of the same phenomenon and hence one-to-one correlation should exist between PD and PVE. However, Ke.Tanaka [44] has experimentally shown that the time constants of the PD and the VE in As_2S_3 are different. It is observed that the PVE saturates earlier than the PD. These experimental observations, on the other hand, suggest that these two phenomena (PD and PVE) are not directly related to each other. However as these measurements were done after switching off the illumination (metastable state), the correlation during illumination remains unclear.

To understand the dynamics of PD and PVE during illumination, *in-situ* measurements have been performed [45-47]. Fig. 12 shows the results of changes of thickness, $\Delta d/d$, with time during and after illumination obtained by *in-situ* measurements of photo-expansion for $\alpha\text{-As}_2\text{S}_3$ films [45,47]. As soon as the light (mercury lamp) is switched on, the thickness increases rather rapidly, reaches a

maximum after approximately 30 s, and then decreases slowly with time. This decrease continues during the rest of the illumination. This behavior of decrease in thickness change *during* illumination is similar to that of the degradation of photocurrent in amorphous chalcogenides [1,27-29]. By turning off the illumination, the thickness decreases slightly. With the passage of time it decays slowly, due to relaxation of the structure, and reaches a metastable state that can be observed as usual PVE, i.e. PVE observed *after* illumination. This decay behavior of PVE (after the illumination is switched off) is found to be very similar to that of the decay of photocurrent [45].

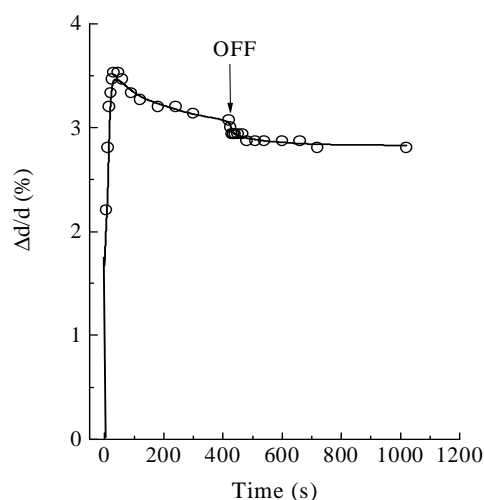


Fig. 12. Relative change in thickness, $\Delta d/d$, with time on switching the illumination and off for obliquely deposited $a\text{-As}_2\text{S}_3$. The solid line is a guide to the eye.

The situation in $a\text{-GeSe}_2$ is different from that in $a\text{-As}_2\text{S}_3$. In Ge-based chalcogenides, volume contraction occurs during and after illumination[45]. In-situ measurement of volume changes clearly show the contraction of $a\text{-GeSe}_2$ films. Surprisingly, however, there is no transient volume changes as observed in $a\text{-As}_2\text{S}_3$ (metastable changes only).

Recent *in-situ* measurement we performed [45], however, is just a primitive and is hard to measure the evolution of PVC in short-time interval. In addition, the spectral analysis of interference fringes is used in this method and hence inaccuracy is involved due to a change in refractive index. A new technique that overcomes the above-mentioned drawback, i.e. a real-time *in-situ* surface height measuring system, has been proposed [48]. In this new technique, the Twyman-Green interferometer [49], fringe phase-shifting method and image analysis technologies [50,51] are employed. The surface height map of the sample is obtained every 1/4 seconds with $\pm 10\text{\AA}$ in accuracy.

Fig. 13 (a) shows an example of surface height map for the flatly deposited $a\text{-As}_2\text{Se}_3$ films (Si substrate) that is obtained by the measuring system described in the previous section. The time evolution of the changes in flatly and obliquely deposited $a\text{-As}_2\text{Se}_3$ is shown in Fig.13 (b) and (c), respectively. In flatly deposited

a-As₂Se₃ film, the surface height increased by 10 nm ($\Delta d/d \approx 2\%$) in 200 seconds of illumination of laser (532 nm in wave length and 91 mW / cm² of power density). After 600 seconds, we turned off the illumination. The surface height started decreasing and settled in 200 seconds at 2 nm less than the height before light off. In case of obliquely deposited *a*-As₂Se₃ film, the surface height decreased by 12 nm ($\Delta d/d \approx 2.4\%$) in 3×10^4 s. The similar results have also been obtained in both obliquely deposited *a*-As₂S₃ and *a*-GeSe₂ films (Si substrate). Fig. 14 shows the time evolution of surface height in flatly deposited *a*-Se onto Si substrate. The height increased rapidly by 2.5 nm ($\Delta d/d \approx 0.5\%$) with illumination ($\lambda = 532$ nm, 91 mW/cm²). As soon as the light was turned off after 800 s of illumination, the height decreased by 2 nm and then gradually decreased to the original height in 200 s.

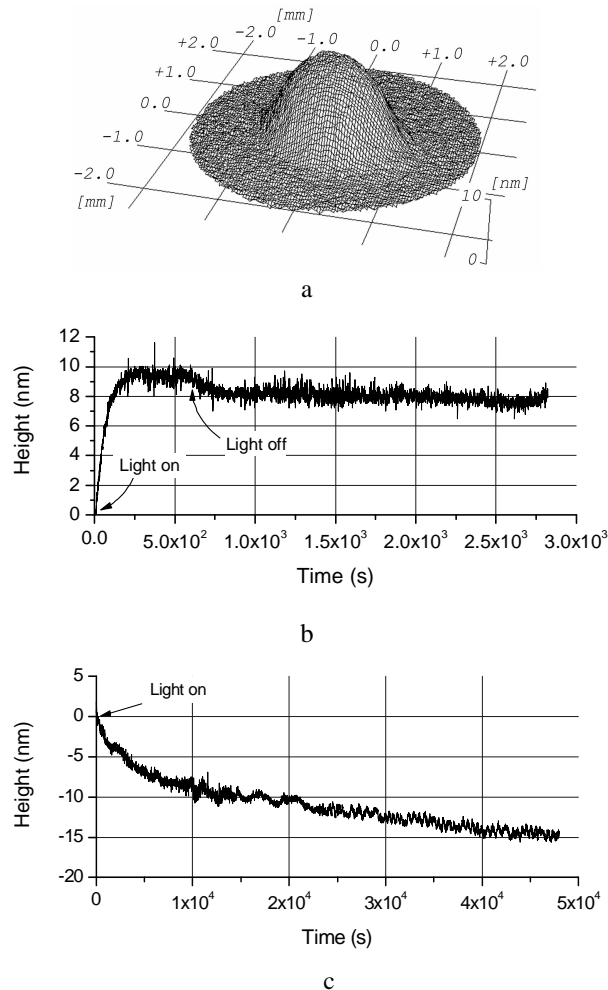


Fig. 13. (a) An example of surface height map for flatly deposited As₂Se₃ film ($\lambda = 532$ nm, 86 mW/cm²). Note that the height scale is enlarged about 10⁵ times of the horizontal scale. (b) Time evolution of the surface height for flatly deposited *a*-As₂Se₃. (c) Time evolution of the surface height for obliquely deposited *a*-As₂Se₃.

Let us discuss the height variations with the illumination. In flatly deposited $a\text{-As}_2\text{Se}_3$ films, as shown in Fig. 13 (b), photoinduced volume expansion (PVE: increase of surface height) is observed during and after illumination. Transient PVE [5] must be involved during illumination, since after illumination is cut off, a slight decrease of the surface height is observed. Remaining increase of surface height after cut off the illumination is so called metastable PVE [5,45]. In obliquely *as-deposited* $a\text{-As}_2\text{Se}_3$ films, as shown in Fig. 13 (c), the surface height increases a little when turning the light on and then decreases with time. The PVE might have been taken over by photoinduced volume contraction and hence the height decreases with time. This volume contraction can be interpreted by void corruption, since many voids are involved in obliquely deposited films which consist of columnar structure with much free space [52]. As the illumination was made in the air, some oxidation may also occur [53].

In the $a\text{-Se}$ films, as shown in Fig. 14, the behaviors are similar to those observed in $a\text{-As}_2\text{Se}_3$ films. Note, however, that the transient PVE in $a\text{-Se}$ is much bigger than that in $a\text{-As}_2\text{Se}_3$. Note also that the transient photodarkening has been reported to be larger in $a\text{-Se}$ than in $a\text{-As}_2\text{Se}_3$ [54].

We have developed the *in-situ* surface height measuring system and have confirmed that it has a good repeatable accuracy to measure the photoinduced volume changes (changes in the surface height). We have reported the transient and metastable volume expansion in the flatly deposited $a\text{-As}_2\text{Se}_3$ and $a\text{-Se}$ films. The same behaviors are observed in $a\text{-As}_2\text{S}_3$ and $a\text{-GeSe}_2$ as well. By prolonged illumination on obliquely deposited $a\text{-As}_2\text{Se}_3$, $a\text{-As}_2\text{S}_3$ and $a\text{-GeSe}_2$, the volume contraction has been observed. This can be due to void corruption in obliquely deposited films. Temperature rise may be involved during illumination and the effect of it should be discussed more carefully.

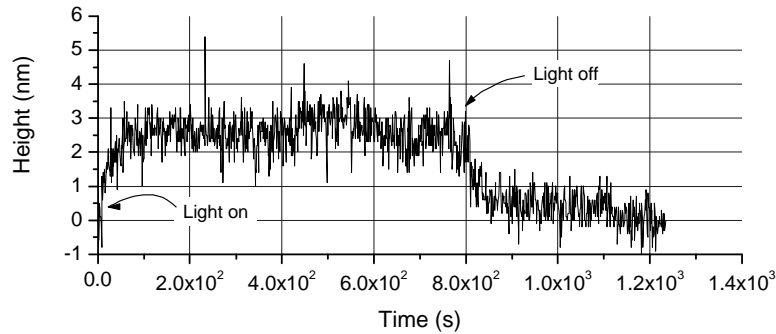


Fig. 14. Time evolution of the surface height with illumination for flatly deposited $a\text{-Se}$ ($\lambda = 532 \text{ nm}$, 86 mW/cm^2).

Photo-induced bandgap changes

In-situ measurements of the optical absorption coefficient have been performed for As_2S_3 [46]. Variation of the changes in absorption coefficient ($\Delta\alpha$) with the number of absorbed photons (n_p), at different temperatures, is shown in Fig. 15. Note that $\Delta\alpha$ is defined as $\Delta\alpha = (-1/d) \ln(\Delta T)$, where d is the film thickness and ΔT the change in optical transmission which is defined here as $\Delta T = T/T_0$ (T_0 is

the transmission when the illumination is put on and T is the transmission at any time t). The details of experimental conditions are described elsewhere [46].

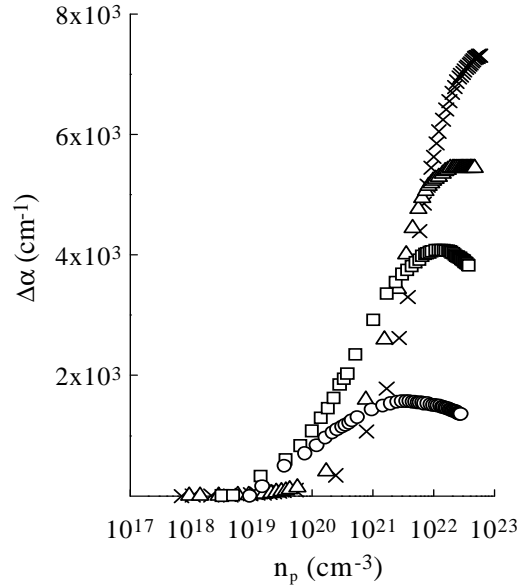


Fig. 15. Variation of changes in absorption coefficient, $\Delta\alpha$, in an obliquely deposited $a\text{-As}_2\text{S}_3$ film as a function of number of absorbed photons n_p at various temperatures. \times , Δ , \square , and \circ show the changes at 50, 100, 200, and 300 K, respectively.

Initially, $\Delta\alpha$ increases slowly with n_p , followed by a large increase and then almost saturation. The magnitude of the changes decreases with increasing temperature with $\Delta\alpha$ being a maximum at 50 K (in spite of a slow initial variation with time or n_p) and smallest at 300 K. At 50 and 100 K, the changes are very slow to start with and increase rapidly as n_p increases, while at 200 and 300 K, there is a more continuous growth of $\Delta\alpha$. The slow initialization at low temperatures is attributed to a smaller number of absorbed photons, as the initial absorption coefficient is small at lower temperatures ($\alpha_0=150\text{ cm}^{-1}$ at 50 K). With increasing time of illumination, the number of absorbed photons rises owing to an increase in the absorption coefficient resulting in a large PD at low temperatures.

Next we show the results of transient photodarkening in $a\text{-As}_2\text{Se}_3$ films (normally deposited). Fig. 16 (a) shows the time evolution of the changes in the absorption coefficient, $\Delta\alpha$, at 1.95 eV during various cycles of Ar laser illumination at 50 and 300 K. The details of the measurements are presented elsewhere [54]. $\Delta\alpha$ increases rapidly at first at both temperatures before reaching close to saturation after some time. When the Ar-laser illumination is switched off, a decrease in $\Delta\alpha$ is observed which reaches a constant value quickly. This portion of the total change is the *transient* part induced by illumination and the portion remaining after stopping the illumination is the usually observed metastable PD. Fig. 16 (b) shows the initial kinetics of $\Delta\alpha$. $\Delta\alpha$ increases and decreases very

rapidly when the illumination is switched on and off, but in neither case does it return the original value, i.e. the metastable photodarkening is accumulated with each successive illumination. The total increase in $\Delta\alpha$, during illumination, is the sum of the transient and the metastable PD. The transient parts of the changes are found to be nearly 60% and 30 % of the total changes induced during illumination at 300 and 50 K, respectively. The cycling was repeated many times after the metastable state was reached, and every illumination confirmed the occurrence of only the transient PD.

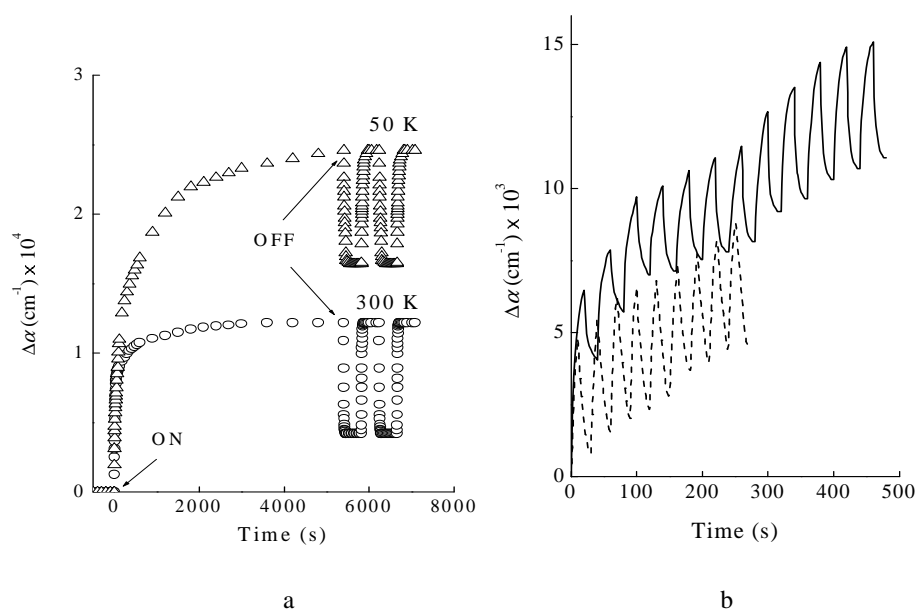


Fig. 16. (a) Time evolution of changes in absorption coefficient, $\Delta\alpha$, for $a\text{-As}_2\text{Se}_3$ films at 50 (Δ) and 300 K (O). ON and OFF stages of the Ar laser are indicated by the arrows. (b) $\Delta\alpha$ with time for short-duration illumination for $a\text{-As}_2\text{Se}_3$ films at 50 (solid line) and 300 K (dashed line).

As already stated, a change in the interaction of chalcogen lone-pair (LP) electrons should be responsible for PD to occur. There are principally three kinds of model: First is the bond-twisting model [4,55]. Understanding of the mechanism of the photostructural changes was the suggestion that changes in positions of atoms without bond breaking can be possible (bond-twisting of Se or S), which may result in a stronger LP-LP interaction, yielding a broadening of the VB, and thus resulting in PD.

Second is the bond-breaking model [56]. Based on the *in-situ* measurements of EXAFS for $a\text{-Se}$ [3,56], the bond alteration model was presented to explain PSC induced by illumination. This idea was presented based on an observed increase in the coordination number by about 5 % in the excited state for $a\text{-Se}$. Associated with the change in coordination, the disorder (mean-square relative displacement) also increases under illumination. After illumination, the local change of coordination disappears whereas the light-induced structural disorder remains (transient effect). This accords with the fact that in $a\text{-Se}$ there is

very small metastable PD [1-4]. The observed increase in the coordination number suggests the formation of 3-fold coordination of Se (a pair of 3-fold neutral sites Se_3^0 - Se_3^0). The formation of inter-chain bonds may induce a local distortion, resulting in an increase in the mean-square relative displacement of the EXAFS spectrum. This bond alternation model is somewhat similar to the model proposed by Elliott [57].

The microscopic models proposed for elemental Se [4,55,56], however, cannot account the occurrence of PVE. For example, a distortion around 3-fold coordination pair itself suggests “contraction” around the network. Probably, overall network changes, which are initiated by bond-twisting or bond alternation, should be taken into consideration in PVE. Both these basic models consider only *particular atoms* that are excited by photoirradiation. The top of valence band is formed by the LP *bands*, and hence there is no reason why particular atoms should be excited selectively. In fact, the bandgap illumination is known to be more effective in inducing PD (localized states are not selectively excited). It is therefore suggested that the “mesoscopic or macroscopic” interaction is dominant for both PD and PVE to occur, because LP electrons have equal probabilities of being excited. Therefore, electrons or holes in the extended states (or band-tail states) can be regarded as being responsible for PD or PVE, but not individual atoms. To induce a large volume changes, macroscopic interaction will be required.

We hence reach the following third model: The repulsion and slip motion of structural layers is proposed (RS model) as shown in Fig. 17 [58]. As a typical example, PD and PVE for $\alpha\text{-As}_2\text{Se}(\text{S})_3$ which is known to have basically layered structures, should be discussed. During illumination, the photocreated electrons should reside mostly in the CB tails, while the photocreated holes diffuse away to the un-illuminated region through VB and VB tails, since the mobility of electrons is much lower than that of holes in amorphous chalcogenides. Thus the layers, which absorb photons, become negatively charged, giving rise to a repulsive Coulomb interaction between layers which produces a weakening of the van der Waals forces, and hence the interlayer distance increases (PVE).

The expansion process is indicated by the arrow E (process E) in Fig. 17. The experimentally observed widening of the valence angle subtended at S atoms within a layer [59] and hence subsequent increase in the distance between two arsenic atoms bridged by a chalcogen atom on illumination can be explained by the repulsive force involved in the process E (dashed arrow); the reaction of repulsive force between layers acts as a compressive force for each layer. Note, however, that the third coordination sphere (As-S-As-S) remains unchanged, which suggests that the dihedral angle between the two adjacent AsS_3 pyramids changes simultaneously with the increase in the valence angle at the bridging chalcogen atom. It is expected, however, that no change in the LP-LP interaction occurs in this process and hence the PD is not induced at this stage.

A slip motion along the layers should also take place with the occurrence of the E process between neighboring clusters. A slip motion is shown by the arrow S (process S). As the energy required for a slip motion along layers is expected to be greater than that for expansion normal to layers, the rate of S motion may be lower than process E. This can be supported by the fact that cleaving is very easy for layered materials, for example graphite.

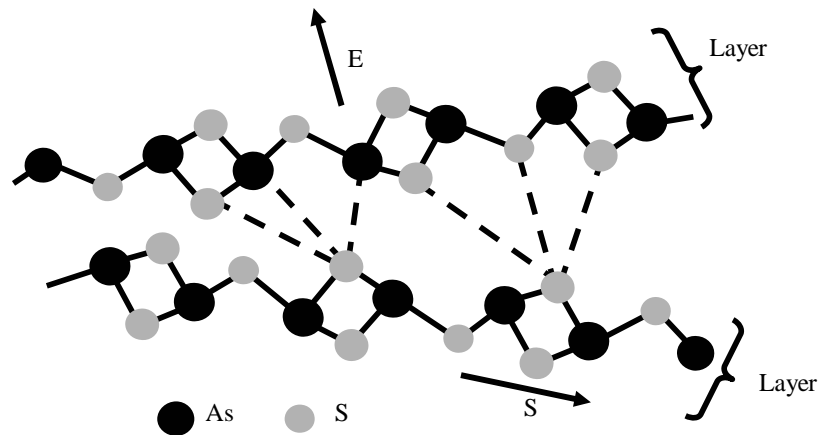


Fig. 17. The repulsion and slip motion of layered cluster model. The arrow E and S indicate the expansion (due to repulsion) and the slip motions, respectively. The difference in local environments (and hence LP interaction) between chalcogen atoms is indicated by the dashed lines.

Both the processes E and S occur owing to the same repulsion force between the layers, but only process S is expected to be directly related to PD [58]. If the neighboring layer slips away from the equilibrium position, an increase in the energy of the highest occupied states (VB) is expected owing to an increase in the total LP-LP interactions. This leads to a widening of the VB, but the CB remains almost unchanged [14], resulting in PD.

The RS model may further be supported by the following experimental results. As already stated, the PD effect disappears in metal-doped chalcogenides [60,61]. This can be explained as follows: atoms of an introduced metals, such as copper, may act as bridging atoms between the layers and hence reduce the flexibility of the layer network. Such bridging will then reduce the ability of both PVE as well as the slip motion. Furthermore, the introduction of such a strong constraint also induces dangling bonds which act as recombination centers and which reduce the number of photo-excited free carriers considerably. We now know that constraint of structural network reduces PD.

As already suggested, one more important factor for structural changes to occur is the *charge separation* during illumination. The RS model predicts also that no PVE and PD can occur in very thin films, because then the photoexcited holes cannot diffuse away from the illuminated region and hence the layer surface area will remain electrically neutral. It was reported, in fact, that no PD can be induced in As_2S_3 films thinner than 50 nm [62].

From the similar spectral dependence between the PD and the photoconductivity in As_2S_3 , and the similar behaviors between PVE and photoconductivity during and after stopping the illumination [45], free-carrier generation but not geminate (excitonic) pairs is suggested to be responsible for the

structural changes, which seems to be consistent with the RS model.

Application of electric field may assist charge separation if the field is properly applied and may enhance PD. It is of interest to examine whether this kind of field effect is found or not. Actually, It is observed that application of an electric field accelerates PD, depending on the magnitude and polarity of the field.

Fig. 18 shows the time evolution of the changes in the absorption coefficient, $\Delta\alpha$, at 1.95 eV (He-Ne laser) [63]. The illuminating light intensity was 100 mW/cm^2 (Ar ion laser). The biasing conditions for an external electric field of $5 \times 10^4 \text{ V/cm}$ (applied voltage 10 V) are as follows: \triangle represents a positive voltage on the ITO (illuminated side), \circ a minus voltage on the ITO, and \square corresponds to zero biasing. Measurements were done in the order \triangle , \circ , and \square . The samples were annealed at 473 K in each cycle of measurements. It was found that the initial transmittance T_0 takes almost the same value, indicating that the PD is reversible. The solid lines are the fittings obtained using the following stretched exponential function:

$$\Delta\alpha = \Delta\alpha_s \left[1 - \exp \left\{ - \left(\frac{t}{\tau} \right)^\beta \right\} \right], \quad (16)$$

where t is the time after the illumination is switched on, τ the effective reaction time, $\Delta\alpha_s$ the saturated value of $\Delta\alpha$, and β is a dispersion parameter ($0 < \beta < 1.0$). The fitting seems to be reasonable and gives values of $\Delta\alpha_s$, τ , and β , all of which will be discussed in the next section.

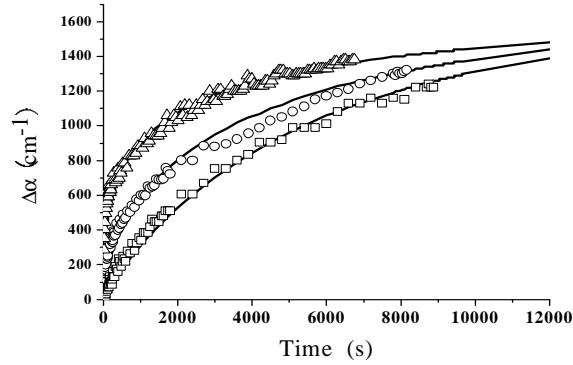


Fig. 18. Time evolution of the changes in the optical absorption coefficient $\Delta\alpha$. \triangle , \circ , and \square represent plus, minus, and zero biasing conditions on ITO (illumination side), respectively. The solid curves are fits obtained using Eq. (16).

Fitting to the experimental data produces the physical parameters, $\Delta\alpha_s$, τ , and β . We tabulate these quantities in Table. It is seen from the Table that the rate of PD, which can be defined as $1/\tau$, increases with electric field, while the saturated value of the PD, $\Delta\alpha_s$, takes almost the same value, irrespective of the presence or absence of the field. This means that under the present biasing condition (5×10^4

V/cm) the saturated number of photodarkened sites is independent of the magnitude of the field, although the presence of the field accelerates photodarkening.

Positive biasing, plus (+) on ITO, which increases the relative concentration of electrons in illuminated area (near the ITO), because holes drift away to the unilluminated counter Au-electrode, shows the highest reaction rate (shortest reaction time). Negative biasing, minus (-) on the ITO, gives an intermediate reaction rate between positive and zero biasing. The number of holes increases with negative biasing as electrons diffuse away to the counter Au electrode. However, as the diffusion coefficient (or drift mobility) of electrons is smaller than that of holes, electronic charging (positive in this case) is expected to be smaller than that for positive biasing. The zero biasing case therefore gives the lowest reaction rate among the three biasing conditions.

To confirm that holes are the more mobile carrier in a-As₂Se₃, the photovoltage (the Dember effect), V_p , has been measured at 300 K under the present conditions (Ar ion laser, 100 mW/cm²). We obtained $V_p = 160$ meV with the expected polarity, i.e. the illuminated ITO electrode is negative and the counter Au electrode is positive, indicating that holes are mobile than electrons. On the other hand the photovoltage can be expressed by [63]

$$V_p \approx \frac{kT}{e} \ln \left(\frac{\sigma_i}{\sigma_d} \right), \quad (17)$$

where σ_i and σ_d are the photoconductivity and dark conductivity, respectively. In the present conditions ($\sigma_i/\sigma_d \approx 10^2$) V_p is estimated to be ~150 meV, which is almost the same value as that obtained experimentally.

Application of moderate electric field shortens the reaction time of the PD, depending on the biasing conditions (polarity) of the electric field, while the magnitude of the PD is the same as that without an electric field. The results suggest that charge separation between photoexcited electrons and holes is a dominant factor in the occurrence of PD. This may support the RS model.

Finally, we should discuss the transient changes of PD and PVE during illumination. The total changes consist of transient and metastable components. The transient component decays when the illumination is switched off and only the metastable PD is observed after cessation of the light. The mechanism can be understood in the following way. Upon absorbing a photon, a “cluster” in the ground state is transferred to the excited state *via* the transient state. The relaxation of the transient state may proceed along two different pathways, either back to the ground state (the transient component) or into the metastable or a new equilibrium state (the metastable component).

Potentiality of device applications

As the ratio, photoconductivity/dark-conductivity for bandgap illumination, in chalcogenide glasses (CGs) is very much large, chalcogenide glasses have been used to photo-sensors, electrophotography (Xerography) etc. Recently, large area x-ray image sensors for a medical purpose, have been developed using a-Se [64,65]. This is due to the fact that enough electron-hole pairs are produced by x-ray exposure. These optoelectronic properties are essential for chalcogenide glasses.

Other important applications using CGs are presented in comprehensive review articles [65-71] and these will be briefly introduced as follows. As the optical transmittance in near- and mid-infrared regions is very high (up to 20 μm , for example, in tellurides), CGs can be useful as optical materials such as lenses, coatings, prisms etc. In rare-earth doped CGs, photoluminescence in the visible, near-IR, and mid-IR regions is found and it can be used as light amplifiers in a fiber form, lasers and sensors. As stated in the present chapter, the exposure of light changes the volume and surface profile. Bragg gratings and micro-lenses can be fabricated from photoresists.

Micro-lenses may have potential applications, for example, as imaging machines, optical communications etc. In particular, sub-gap illumination to CGs is very efficient for fabricating Bragg gratings, self-focusing microlenses, inducing “network fluidity” [67]. Optically induced fluidity may lead to a optomechanical effect. In contrast to piezo-electric actuators, highly reversible and non-hysteristic actuators were realized and these are potentially cheap and easy to fabricate. In this actuator, it is confirmed that the light energy is directly converted into mechanical work [68].

Optical data storage, for example, known as DVD (digital versatile discs), appeared in a big market already. The present DVDs are the “phase-change overwrite (million times!)” discs using Ge-Te-Sb system [69]. This type of consumer-use rewritable phase-change optical disc became the mainstream of the optical disc world. Optical discs with dramatically increased density (240 Gbit/in²) and data-processing (Tbit/s) are expected in near future. A super-resolution near-field structure of optical storage devices using Ge-Sb-Te system has been also proposed [70]. There is also a comprehensive review for integrated optics applications using CGs, in which importance of CGs are emphasized as engineering glassy materials [71].

Summary

Current understandings of the optoelectronic properties in amorphous chalcogenides were briefly reviewed in this chapter.

Fundamental optical absorption in amorphous chalcogenides is not always expressed by well-known Tauc’s relation, which has been overcome by introducing the density-of-states in fractal structures of amorphous chalcogenides. Fractal nature may be originate from clustered layer structures.

The electronic conductivity is also not expressed by the standard band-transport model. The conductivity prefactor takes very small values, which is not easy to be predicted from the standard theory, and it correlates with the activation energy. This correlation is called the Meyer-Neldel rule (MNR), while its origin is not clear. The small prefactor suggests that the transport occurs between clustered layers. Such potential barriers between clusters prevents complete band transport.

The dynamics of photo-induced defect creation, volume changes (in particular photo-induced volume expansion; PVE), and photodarkening (PD) for amorphous chalcogenides, were also discussed. The quantum efficiency of light-induced creation of metastable defects in a-As₂Se₃ for bandgap and sub-gap illumination has been estimated from the photocurrent measurements. A higher quantum efficiency even for sub-gap illumination has been observed, suggesting

that self-trapped excitons may initiate LIMD creation. It has been also found that the defect creations are larger for obliquely deposited films compared to normally deposited films, which can be due to larger flexibility of obliquely deposited films with many voids. This leads to a larger value of quantum efficiency of light-induced defect creation in obliquely deposited films.

Time evolutions of PVE and PD (*in-situ* measurements) were performed. During illumination, the total changes constitute transient and metastable effects. The transient changes decay when the illumination is switched off to give the usually observed metastable photodarkening or expansion. Further illumination, after the metastable state is reached, induces only transient changes. The origin of PVE and PD was discussed in terms of the model of repulsion and slip motion of clustered layers.

Fundamental optical and electronic properties and photoinduced metastabilities can be dominated by the existence of clustered layer structures in chalcogenide glasses. Through this chapter, we emphasized that this rather macroscopic viewpoint can be important to understand overall natures observed in chalcogenide glasses.

Acknowledgements

The authors would like to thank Ted Davis, Takeshi Aoki, Keiji Tanaka, and Astosh Ganjoo for many suggestions and discussions. We also thank to J. Hegedus and K. Kohary for their collaboration in structural simulation works. The part of computer simulation work has been done using a computer in Tokyo Polytechnic University. The present work has been supported by a Grant-in-Aid for scientific research (2002, 2003) from the Ministry of Education in Japan, the OTKA Fund (Grant No. T043231), and by Hungarian-British and Hungarian-Japanese intergovernmental S and T Programmes (No. GB-17/2003 and No. JAP-7/2000).

References

- [1] K. Shimakawa, A. V. Kolobov, S. R. Elliott, *Adv. Phys.* **44**, 475 (1995).
- [2] Koichi Shimakawa, *Dynamics of Photo-induced Metastability in Amorphous Chalcogenides*, edited by A.V. Kolobov (Wiley-VCH GmbH & Co. KGaA, Weinheim, 2003) p.58.
- [3] A. V. Kolobov, K. Tanaka, *Handbook of Advanced Electronic and Photonic Materials and Devices Vol.5*, edited by H.S. Nalwa (Academic Press, San Diego, 2001) p.47.
- [4] Ke. Tanaka, *Rev. Solid St. Sci.* **4**, 641 (1990).
- [5] Jai Singh, Koichi Shimakawa, *Advances in Amorphous Semiconductors* (Taylor and Francis, London and New York, 2003).
- [6] Mehrun Nessa, K. Shimakawa, A. Ganjoo, J. Singh, *J. Optoelectron. Adv. Mater.* **2**, 133 (2000).
- [7] K. Shimakawa, F. Abdel-Wahab, *Appl. Phys. Lett.* **70**, 652 (1997).
- [8] J. Tauc, *The Optical Properties of Solids*, edited by F. Abeles (North-Holland, Amsterdam, 1979) p.277.
- [9] N. F. Mott, E. A. Davis, *Electronic Processes in Non-Crystalline Materials* (Clarendon Press, Oxford, 1979)

- [10] B. B. Mandelbrot, *The Fractal Geometry of Nature* (Freeman, New York, 1982).
- [11] R. Zallen, *The Physics of Amorphous Solids* (John Wiley & Sons, New York, 1983) p.135.
- [12] S. R. Elliott, *The Physics of Amorphous Semiconductors* 2nd ed. (Longman Scientific & Technical, London, 1990).
- [13] Ke. Tanaka, *Jpn. J. Appl. Phys.* **37**, 1747 (1998).
- [14] Y. Watanabe, H. Kawazoe, M. Yamane, *Phys. Rev. B* **38**, 5677 (1988).
- [15] Jai. Singh, T. Aoki, K. Shimakawa, *Philos. Mag. B* **82**, 855 (2002).
- [16] Xing-Fei He, *Phys. Rev. B* **42**, 11751 (1990).
- [17] U. Dersh, M. Grunnewald, H. Overhof, P. Thomas, *J. Phys. C: Solid State Physics.* **20**, 121 (1987).
- [18] W. Meyer, H. Neldel, *Z. Tech. Phys. (Leipzig)* **12**, 588 (1937).
- [19] A. Yelon, B. Movaghar, *Phys. Rev. Lett.* **65**, 618 (1990).
- [20] A. Yelon, B. Movaghar, M. H. Branz, *Phys. Rev. B* **46**, 12244 (1992).
- [21] J. Fortner, V. G. Karpov, M-L. Saboungi, *Appl. Phys. Lett.* **66**, 997 (1995).
- [22] H. Overhof, P. Thomas, *Electronic Transport in Hydrogenated Amorphous Semiconductors* (Springer, Berlin, 1989) p.122.
- [23] Z.U. Borisova, *Glassy Semiconductors* (Plenum, New York, 1981).
- [24] D. Emin, C. H. Seager, R. K. Quinn, *Phys. Rev. Lett.* **28**, 813 (1972).
- [25] G. Kemeny, B. Rosenberg, *J. Chem. Phys.* **52**, 4151 (1970).
- [26] K. Shimakawa, Meherun-Nessa, H. Ishida, A. Ganjoo, *Philos. Mag.* **84**, 81 (2004).
- [27] K. Shimakawa, S. Inami, S. R. Elliott, *Phys. Rev. B* **42**, 11857 (1990).
- [28] K. Shimakawa, S. Inami, T. Kato, S. R. Elliott, *Phys. Rev. B* **46**, 10062 (1992).
- [29] Meherun Nessa, K. Shimakawa, Ashtosh Ganjoo, *J. Optoelectron. Adv. Mater.* **4**, 93 (2002).
- [30] M. Stutzmann, W. B. Jackson, C. C. Tsai, *Phys. Rev. B* **32**, 23 (1985).
- [31] K. Morigaki, *Jpn. J. Appl. Phys.* **28**, L2128 (1989).
- [32] K. Imagawa, K. Shimakawa, A. Kondo, *J. Non-Cryst. Solids* **266-269** (2000).
- [33] M. Stutzmann, J. Nunnenkenkamp, M. S. Brandt, A. Asano, *Phys. Rev. Lett.* **67**, 2347 (1991).
- [34] J. Hegedus, Diploma Thesis, Budapest University of Technology and Economics (2003).
- [35] J. Hegedus, K. Kohary, S. Kugler, K. Shimakawa, *J. Non-Cryst. Solids* (to be published in 2004).
- [36] K. Kohary, S. Kugler, *Phys. Rev. B* **63**, 193404 (2001).
- [37] K. Kohary, S. Kugler, *J. Non-Cryst. Solids* **266-269**, 746 (2000).
- [38] J. Hegedus, K. Kohary, S. Kugler, *J. Non-Cryst. Solids* (to be published in 2004).
- [39] D. Molina, E. Lomba, G. Kahl, *Phys. Rev. B* **60**, 6372 (1999).
- [40] E. Lomba, D. Molina, M. Alvarez, *Phys. Rev. B* **61**, 9314 (2000).
- [41] F. Shimojo, K. Hoshino, Y. Zempo, *J. Phys. C: Condens. Matters* **10**, L177 (1988).
- [42] Y. Kuzukawa, Ashtosh Ganjoo, K. Shimakawa, *J. Non-Cryst. Solids* **227-230** 715 (1998).
- [43] Y. Kuzukawa, Ashtosh Ganjoo, K. Shimakawa, Y. Ikeda, *Philos. Mag. B* **79**, 249 (1999).
- [44] Ke. Tanaka, *Phys. Rev. B* **57**, 5163 (1998).
- [45] Ashtosh Ganjoo, Y. Ikeda, K. Shimakawa, *Appl. Phys. Lett.* **74**, 2119 (1999);

- J. Non-Cryst. Solids **266-269**, 919 (2000).
- [46] Ashtosh Ganjoo, K. Shimakawa, H. Kamiya, E. A. Davis, Jai Singh, Phys. Rev. B **62**, R14601 (2000).
- [47] Ashtosh Ganjoo, K. Shimakawa, J. Optoelectron. Adv. Mater. **4**, 595 (2002).
- [48] Y. Ikeda, K. Shimakawa, J. Non-Cryst. Solids (to be published in 2004).
- [49] M. Born, E. Wolf, *Principles of Optics 7th (Expanded) Edition* (Cambridge University Press, Cambridge, 1999) p.336.
- [50] J. E. Greivenkamp, J. H. Bruning, *Optical Shop Testing*, ed. D. Malacara (Wiley, New York, 1992) Chap. 14.
- [51] P. D. Groot, Appl. Opt. Vol. **34** No. 22 (1995) 4723. [48].
- [52] S. Rajagopalan, K. S. Harshavardhan, L. K. Malhotra, K. L. Chopra, J. Non-Cryst. Solids **50**, 29 (1982).
- [53] C. A. Spence, S. R. Elliott, Phys. Rev. B **39**, 5452 (1989).
- [54] Astosh Ganjoo, K. Shimakawa, K. Kitano, E. A. Davis, J. Non-Cryst. Solids **299-302** (2002) 917.
- [55] Ke. Tanaka, J. Non-Cryst. Solids, **35&36**, 1023 (1980); Philos. Mag. Lett. **79**, 25 (1999).
- [56] A. V. Kolobov, H. Oyanagi, K. Tanaka, Ke. Tanaka, Phys. Rev., B **55**, 726 (1997).
- [57] S. R. Elliott, J. Non-Cryst. Solids, **81**, 71 (1986).
- [58] K. Shimakawa, N. Yoshida, A. Ganjoo, A. Kuzukawa, J. Singh, Philos. Mag. Lett. **77**, 153 (1998).
- [59] C. Y. Yang, M. A. Paesler, D. E. Sayers, Phys. Rev. B **36**, 9160 (1987).
- [60] J. Z. Liu, P. C. Taylor, Phys. Rev. Lett. **59**, 1938 (1987); Phys. Rev. B **41**, 3163 (1990).
- [61] M. Iovu, S. Shutov, S. Rebeja, E. Colomeyco, M. Popescu, J. Optoelectron. Adv. Mater. **2**, 53 (2000).
- [62] K. Hayashi, N. Mitsuishi, J. Non-Cryst. Solids **299-302**, 949 (2002).
- [63] K. Shimakawa, T. Kato, T. Hamagishi, J. Non-Cryst. Solids (in print).
- [64] J. A. Rowlands, S. O. Kasap, Physics Today **50**, 24 (1997).
- [65] S. O. Kasap, J. A. Rowlands, *Thin Film Materials and Devices-Development in Science and Technology*, ed. By J.M. Marshall, N. Kirov, A. Vabrek, and J.M. Maud (World Scientific, Singapore, 1999) p.13.
- [66] M. Frumar, B. Frumarova, T. Wagner, P. Nemeč, *Photo-induced Phenomena in Amorphous and Glassy Chalcogenides*, edited by A.V. Kolobov (Wiley-VCH GmbH & Co.KGaA, Weinheim, 2003) p.23.
- [67] Ke. Tanaka, *Sub-gap Photo-induced Phenomena in Chalcogenide Glasses*, A. V. Kolobov (Wiley-VCH GmbH & Co.KGaA, Weinheim, 2003) p.69.
- [68] M. Stuchlik, P. Krecmer, S. R. Elliott, *The Optomechanical Effect in Amorphous Chalcogenide Films*, A. V. Kolobov (Wiley-VCH GmbH & Co.KGaA, Weinheim, 2003) p.109.
- [69] T. Ohta, S. R. Ovshinsky, *Phase-Change Optical Storage Media*, A. V. Kolobov (Wiley-VCH GmbH & Co.KGaA, Weinheim, 2003) p.310.
- [70] J. Tominaga, *Application of Ge-Sb-Te Glasses for Ultrahigh-Density Optical Storage*, A.V. Kolobov (Wiley-VCH GmbH & Co.KGaA, Weinheim, 2003) p.327.
- [71] K. Richardson, T. Cardinal, M. Richardson, A. Schulte, S. Seal, *Engineering Glassy Chalcogenide Materials for Integrated Optics Applications*, A. V. Kolobov (Wiley-VCH GmbH & Co.KGaA, Weinheim, 2003) p. 383.